ARTICLE NO. 78-1136R

Numerical Solution of the Supersonic and Hypersonic Viscous Flow around Thin Delta Wings

Guion S. Bluford Jr.*
Air Force Flight Dynamics Laboratory, Wright-Patterson Air Force Base, Ohio

Numerical solutions have been obtained for the supersonic and hypersonic viscous flowfields around thin planar delta wings. These solutions were obtained by solving the unsteady Navier-Stokes equations subject to a conical approximation. The integration technique used was MacCormack's explicit finite-difference scheme. Solutions were obtained for the upper, lower, and total flowfields around delta wings with supersonic leading edges. These solutions span a Mach number range of 2.94 to 10.16, a local Reynolds number range of 3.345×10^5 to 5.0×10^6, and various angles of attack from − 15 deg to + 15 deg. The numerical results compare quite favorably with both supersonic and hypersonic experimental flowfield data. This investigation demonstrated the feasibility of applying a conical approximation to the Navier-Stokes equations in order to calculate the flow around thin delta wings.

Nomenclature

a = local speed of sound
c = adjustable constant for maximum time step
Def = deformation tensor
e = total specific internal energy
F,G,H = vector fluxes
i,j = indexes of the grid system
$\bar{\bar{I}}$ = unit identity matrix
M = Mach number
p = static pressure
Pr = Prandtl number
$\dot{q}$ = rate of heat transfer
r = radial coordinate
Re = Reynolds number
t = time
T = static temperature
U = vector of the dependent variables
u,v,w = velocity components in Cartesian frame
x_m,x_i = tensor form of Cartesian coordinates
x,y,z = Cartesian coordinates
α = angle of attack
γ = ratio of specific heats (1.40 for air)
γ_c = cross-flow vector angle with postive η axis
Δ = incremental value
ξ,η,ζ = transformed coordinate system
$\xi_{x_m},\eta_{x_m},\zeta_{x_m}$ = coordinate transformation derivatives
θ = conical angle
λ = second coefficient of viscosity
μ = absolute viscosity
ρ = density
Σ = summation notation
$\bar{\bar{\tau}}$ = stress tensor
$\bar{\bar{\tau}}'$ = viscous stress tensor $\bar{\bar{\tau}}' = \bar{\bar{\tau}} + p\bar{\bar{I}}$
ϕ = circumferential angle
Φ = dissipation function
$\bar{\chi}$ = hypersonic similarity parameter

Superscripts

$-$ = vector
$=$ = tensor
n = time step level

Subscripts

i = tensor coordinate indexes
i,j = indexes of the grid system
m = coordinate indexes 1, 2, 3
max = maximum value
o = stagnation condition
w = surface or wall conditions
DF = diffusion part of linearized Navier-Stokes equations
INV = inviscid part of linearized Navier-Stokes equations
MXD = mixed-derivative part of linearized Navier-Stokes equations
∞ = freestream condition

I. Introduction

AERODYNAMICISTS have been investigating the supersonic and hypersonic flowfields around delta wings for a number of years.[1-3] Recent development of the Space Shuttle has focused renewed interest and increased research activity in this area. Previous efforts at studying this problem were directed towards analyzing the lower surface or compression side of the flowfield. However, from recent experiments, it was seen that the most striking features of the flow exist in the upper surface or leeside flowfield. At angle of attack, an embedded shock is formed on the expansion side of the delta wing. The interaction of this embedded shock wave with the attached boundary layer can create vortices in the boundary layer at low angles of attack and flow separation at large angles of attack.[4] Both of these features increase the temperature and pressure gradients on the upper surface of the wing. Previous analytical and numerical studies have addressed only the inviscid supersonic and hypersonic flows around delta wings.[5-9] No satisfactory solution has been found which can calculate the induced vortex phenomena within the boundary layer and the shock-induced separation on the upper surface.[3]

In this study, a unique technique is used to solve both the inviscid and viscous flows around thin delta wings. This technique involves solving the Navier-Stokes equations subject to a conical approximation.[10] The delta wings used in

---

Received July 6, 1978; presented as Paper 78-1136 at the AIAA 11th Fluid and Plasma Dynamics Conference, Seattle, Wash., July 10-12, 1978; revision received March 26, 1979.

Index categories: Supersonic and Hypersonic Flow; Aerodynamics.

*Major, U.S. Air Force, Astronaut Candidate, Johnson Space Center, Houston, Texas. Member AIAA.

this investigation have supersonic leading edges with laminar boundary layer flows. Solutions are obtained for both the upper and lower surface flowfields at various angles of attack, Mach numbers, and Reynolds numbers. These numerical results show for a first time the shock-induced vortex development within the boundary layer and also provide good agreement with the experimental data of Bannink et al.,[11] Cross,[12] and Spurlin.[13] These solutions provide a unique insight and an improved understanding into the dynamics of this complex flowfield phenomena.

II. Governing Equations

The unsteady, compressible, three-dimensional Navier-Stokes equations can be written in conservative form as follows:

$$\frac{\partial \rho}{\partial t} + \nabla \cdot (\rho \bar{u}) = 0 \tag{1a}$$

$$\frac{\partial (\rho \bar{u})}{\partial t} + \nabla \cdot (\rho \bar{u}\bar{u} - \bar{\bar{\tau}}) = 0 \tag{1b}$$

$$\frac{\partial (\rho e)}{\partial t} + \nabla \cdot (\rho e \bar{u} - \bar{u} \cdot \bar{\bar{\tau}} + \dot{\bar{q}}) = 0 \tag{1c}$$

where the heat flux is defined as $\dot{\bar{q}} = -k \nabla T$, the viscous dissipation function Φ is $\bar{\Phi} = \bar{u} \cdot \bar{\bar{\tau}}$, and the stress tensor is

$$\bar{\bar{\tau}} = -p\bar{\bar{I}} + \lambda(\nabla \cdot \bar{u})\bar{\bar{I}} + \mu \text{ Def } \bar{u} \tag{2}$$

The equation of state, Sutherland's viscosity formula, and a fixed Prandtl number (0.72) provide a closed system of governing equations.

A generalized body-oriented coordinate transformation is used to map the physical plane (x,y,z) into the transformed plane (ζ,η,ξ). In this study, the generalized coordinate transformation is introduced as

$$\zeta = \zeta(r) \quad \eta = \eta\left(\frac{y}{x}, \frac{z}{x}\right) \quad \xi = \xi\left(\frac{y}{x}, \frac{z}{x}\right) \tag{3}$$

where

$$r = \sqrt{x^2 + y^2 + z^2}$$

The governing equations to be solved in this transformed domain are written as follows:

$$\frac{\partial U}{\partial t} + \sum_m \zeta_{x_m} \frac{\partial F_m}{\partial \zeta} + \sum_m \eta_{x_m} \frac{\partial G_m}{\partial \eta} + \sum_m \xi_{x_m} \frac{\partial H_m}{\partial \xi} = 0 \tag{4}$$

where $m = 1, 2, 3$; the ξ_{x_m}, η_{x_m}, and ξ_{x_m} denote the first-order partial derivatives of the transformed independent variables (ζ,η,ξ) with respect to the Cartesian coordinates (x,y,z). The vector fluxes, U, F_m, G_m, and H_m are defined as

$$U = \left| \begin{matrix} \rho \\ \rho u \\ \rho v \\ \rho w \\ \rho e \end{matrix} \right| \tag{4a}$$

$$F_1 = G_1 = H_1 = \left| \begin{matrix} \rho u \\ \rho u u - \tau_{xx} \\ \rho u v - \tau_{xy} \\ \rho u w - \tau_{xz} \\ \rho e u + \dot{q}_x - \phi_x \end{matrix} \right| \tag{4b}$$

$$F_2 = G_2 = H_2 \left| \begin{matrix} \rho v \\ \rho v u - \tau_{xy} \\ \rho v v - \tau_{yy} \\ \rho v w - \tau_{yz} \\ \rho e v + \dot{q}_y - \phi_y \end{matrix} \right| \tag{4c}$$

$$F_3 = G_3 = H_3 = \left| \begin{matrix} \rho w \\ \rho w u - \tau_{xz} \\ \rho w v - \tau_{yz} \\ \rho w w - \tau_{zz} \\ \rho e w + \dot{q}_z - \phi_z \end{matrix} \right| \tag{4d}$$

These equations are nondimensionalized by using a characteristic length, the freestream total pressure and density, and by using the maximum adiabatic freestream velocity. This results in a set of normalized governing equations which are functions of the freestream Reynolds number and a characteristic length determined by the Reynolds number.

In this investigation, a conical approximation is applied to the governing equations. Experimental data reveal a conical behavior for flows downstream of the apex region of a delta wing $[\bar{\chi} \leq 0(1)]$ even when viscous effects are present.[11-14] When this requirement is imposed on the governing equations, it is assumed that the gradients in the radial direction are much smaller than those in the crossflow directions (θ,ϕ). Hence,

$$\frac{\partial}{\partial r} << \frac{\partial}{r\partial\theta} \qquad \frac{\partial}{\partial r} << \frac{\partial}{r\partial\phi} \tag{5}$$

This is the mathematical definition of a locally conical flow. Gradients do exist in the radial direction, but they are sufficiently small to be neglected. When this requirement is imposed on the generalized transformed coordinates it becomes

$$\frac{\partial}{\partial \zeta} << \frac{\partial}{\partial \eta} \qquad \frac{\partial}{\partial \zeta} << \frac{\partial}{\partial \xi} \tag{6}$$

Thus, the flow properties $\rho,u,v,w,p,$ and T are nearly invariant along rays from the apex. However, it should be noted that the Reynolds number and the transformed derivatives are functions of ζ and, thus, a characteristic length is included in the computation.

By applying this conical approximation to the conservative form of the governing equations, the resulting equation set becomes:

$$\frac{\partial U}{\partial t} + \frac{\partial}{\partial \eta} \sum_m \eta_{x_m} \frac{\partial G_m}{\partial \eta} + \frac{\partial}{\partial \xi} \sum_m \xi_{x_m} \frac{\partial H_m}{\partial \xi} + \bar{H} = 0 \tag{7}$$

where

$$\bar{H} = -\sum_m G_m \frac{\partial}{\partial \eta}\left(\frac{\partial \eta}{\partial x_m}\right) - \sum_m H_m \frac{\partial}{\partial \xi}\left(\frac{\partial \xi}{\partial x_m}\right) + \sum_m \zeta_{x_m} \frac{\partial F_m}{\partial \zeta}$$

It should be noted that although the primitive variables are constant along lines of constant ζ, the gradients of the stress terms and the coordinate transformations are not zero.

III. Numerical Procedure

The system of equations is solved by using the MacCormack[15] finite-difference scheme with a shock-capturing technique. In this algorithm, forward differences are used in the predictor step to approximate

$$\frac{\partial}{\partial\eta}\sum_m \eta_{x_m}\frac{\partial G_m}{\partial\eta} \qquad \frac{\partial}{\partial\xi}\sum_m \xi_{x_m}\frac{\partial H_m}{\partial\xi} \tag{8}$$

while backward differences are used for these terms in the corrector step.

In order to evaluate the shear stress and heat flux terms appearing in the G_m and H_m matrices, backward differences are used in the predictor step and forward differences in the corrector step. A central difference operator is used for τ_{ij} and $\dot{q}_j$ in the $\bar{H}$ matrix. This differencing procedure results in a central difference approximation with second-order accuracy for all shear stress and heat flux terms.

A generalized stability criteria analysis was performed on the finite-difference form of the simplified Navier-Stokes equations. This analysis, first suggested by MacCormack and Baldwin,[16] accounts for both the inviscid and viscous dominant regions. The maximum allowable time step, in tensor form, is estimated to be

$$\Delta t_{\max} \le c \Big/ \left(\frac{1}{\Delta t_{\mathrm{INV}}} + \frac{1}{\Delta t_{\mathrm{DF}}} + \frac{1}{\Delta t_{\mathrm{MXD}}}\right) \tag{9}$$

where

$$\Delta t_{\mathrm{INV}} = \left[\left|u_i\frac{\partial\eta}{\partial x_i}\right|\left(\frac{1}{\Delta\eta}\right) + \left|u_i\frac{\partial\xi}{\partial x_i}\right|\left(\frac{1}{\Delta\xi}\right)\right.$$
$$+ a\left(\frac{\partial\eta}{\partial x_i}\frac{\partial\eta}{\partial x_i}\frac{1}{(\Delta\eta)^2} + \frac{\partial\xi}{\partial x_i}\frac{\partial\xi}{\partial x_i}\frac{1}{(\nabla\xi)^2}\right.$$
$$\left.\left. + 2\left(\frac{\partial\eta}{\partial x_i}\right)\left(\frac{\partial\xi}{\partial x_i}\right)\frac{1}{\Delta\eta\Delta\xi}\right)^{1/2}\right]^{-1} \tag{9a}$$

$$\Delta t_{\mathrm{DF}} = \frac{\rho Pr\ Re}{\gamma}\left[\left(\frac{\partial\xi}{\partial x_i}\right)\left(\frac{\partial\xi}{\partial x_i}\right)\frac{1}{(\Delta\xi)^2}\right.$$
$$\left. + \left(\frac{\partial\eta}{\partial x_i}\right)\left(\frac{\partial\eta}{\partial x_i}\right)\frac{1}{(\Delta\eta)^2}\right]^{-1} \tag{9b}$$

$$\Delta t_{\mathrm{MXD}} = (12\rho\ Re\ \Delta\eta\ \Delta\xi)\Big/\left(7\frac{\partial\eta}{\partial x_i}\frac{\partial\xi}{\partial x_i}\right.$$
$$\left. + \sqrt{\frac{\partial\eta}{\partial x_i}\frac{\partial\eta}{\partial x_i} + \frac{\partial\xi}{\partial x_j}\frac{\partial\xi}{\partial x_j}}\right) \tag{9c}$$

$$c \le 1.0 \tag{9d}$$

This time step size was only calculated at the beginning of each run and was used until a converged solution (change of $< 10^{-5}$ of each primitive variable) was attained.

Two numerical smoothing schemes were incorporated in the numerical procedure. The fourth-order density damping terms, developed by Tannehill et al.[17] was adopted with modifications. Instead of using a rigorous transformation of the second-order derivatives of density into the transformed space, the second-order derivatives were approximated by the derivatives with respect to the transformed independent variables (η,ξ). The net result is an artificial viscosity-like term of the form

$$-\alpha_m \Delta t(\Delta\xi_m)^3\frac{\partial}{\partial\xi_m}\left(\frac{\partial^2\rho}{\partial\xi_m^2}\frac{\partial U}{\partial\xi_m}\right) \qquad m=2,3 \tag{10}$$

added to the difference equations. This damping term is only of significance in regions of large density oscillations where the truncation error is already degrading the computation. Additionally, normal stress damping, developed by McRae,[10] was also used. This damping technique applies a negative multiplier to the second coefficient of molecular viscosity to smooth out the starting transients within the flow. As soon as these abnormal initial transients decay, the second coefficient of viscosity is reset to Stoke's value and the calculations are continued to a steady-state solution. The magnitude of all these damping terms are set so as to be effective in the inviscid flow region but not to change the viscous region behavior or modify the effective Reynolds number appreciably.

IV. Coordinate System and Boundary Conditions

The body-fixed coordinate system used in this investigation is shown in Fig. 1. The coordinate transformation is defined as follows

$$\zeta = x \quad \eta = y/x \quad \xi = z/x \tag{11}$$

where x is the characteristic length or distance from the apex of the delta wing to the measurement plane. The mesh spacing in the computational domain (η,ξ) is uniformly distributed in both coordinate directions. The viscous effects, in this computational plane, are scaled based on the local Reynolds number.

The computational domain is initialized with freestream conditions at all points except on the body surface. The boundary conditions on the wing surface are

$$u = v = w = 0 \quad \text{at } \eta \le \eta_{\text{wing tip}} \text{ and } \xi = 0 \tag{12a}$$

$$T = T_w \quad \text{at } \eta \le \eta_{\text{wing tip}} \text{ and } \xi = 0 \tag{12b}$$

These expressions satisfy the no-slip velocity requirements and the experimentally determined isothermal conditions. The pressure distribution on the wing is obtained by evaluating the ξ momentum equation at the wing surface. The derivatives contained in this momentum equation are approximated by second-order, one-sided finite differences. Once the pressure is obtained, the density is determined through the equation of state. The leading edge singularity is treated as a triple-valued point with upper, side, and lower pressure and density values. These leading-edge pressures are determined by the normal (η and ξ) momentum equations. The three values of density are calculated from the equation of state.

A symmetry plane exists in the computational domain at $\eta = 0$. The boundary conditions on this symmetry plane are defined as

$$\frac{\partial u}{\partial\eta} = 0 \quad v = 0 \quad \frac{\partial w}{\partial\eta} = 0 \tag{13a}$$

$$\frac{\partial\rho}{\partial\eta} = 0 \quad \frac{\partial T}{\partial\eta} = 0 \tag{13b}$$

The finite-difference "reflection" method is used to calculate and model the primitive variables along the centerline plane.

The freestream boundary conditions are applied on the extremities of the computational domain. The flow through these boundaries is supersonic with respect to the transformed coordinates. Under these conditions, the flow variables at the exterior grid points are set equal to the freestream conditions and are held fixed throughout the entire integration process.

V. Numerical Results

Several different delta wing flowfield problems were solved in this investigation. These included supersonic and hypersonic flows over the leeside of a planar delta wing, supersonic flow over the compression side of a planar delta wing, and

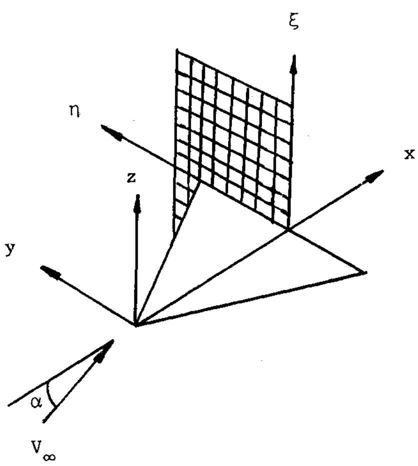

Fig. 1 Coordinate system and computational mesh for delta wing.

finally supersonic and hypersonic flows around thin planar delta wings. All of these solutions are documented in Ref. 22; however, in this paper only three specific cases will be discussed in detail. These include supersonic flowfield cases for both the expansion and compression sides of a delta wing and a hypersonic flowfield case around a thin planar delta wing.

In this analysis, two simplifying assumptions were made in modeling the flow. These were 1) to assume the flows above and below the wing surface are independent of each other and 2) to neglect some of the three-dimensional flowfield effects in the immediate vicinity of the wing vertex and around the leading edge of the wing. Both of these simplifications were applied to the expansion-side-only and compression-side-only solutions; however, only the second one was used in solving the total (upper and lower combined) flowfield.

Expansion Side Flowfield Solution

In order to illustrate an expansion-side-only solution, a supersonic flowfield case was selected. The freestream conditions chosen for this calculation are

$M_\infty = 2.94$ $T_{0_\infty} = 544°\mathrm{R}$

$Re_x = 2.64 \times 10^6$ $P_{0_\infty} = 96$ psia

$Pr = 0.72$ $T_w = 199.5°\mathrm{R}$

where the Reynolds number is based on a root chord length of 0.173 ft. These flowfield parameters correspond identically to those used by Bannink and Nebbeling[11] in their experimental investigation.

The computational domain, on which these calculations were made, consisted of a $26(\eta) \times 30(\xi)$ gird array, similar to the upper half of the grid system shown in Fig. 1. For a wing sweep angle of 45.3 deg, the η step size was 0.063158 with 14 grid points on the wing surface. In the ξ direction, a constant, but different, step size was used for each measurement height (pitot pressure measurements by Bannink[11]) so that experimental and numerical results could be compared without interpolation. These constant step sizes ranged from 0.02393 to 0.02775 for different calculations. The results of these calculations are shown in Figs. 2-6.

In Figs. 2 and 3, several spanwise pitot pressure distributions are shown for various heights above the delta wing. The numerical results of this technique are compared with the inviscid calculations by Kutler[9] and the experimental measurements by Bannink and Nebbeling.[11] For $\xi = 0.0718$ (Fig. 2), the experimental pitot pressure profile across the inboard shock is clearly affected by the interference with the boundary layer. At this height, the measured shock strength is slightly less than that measured at higher values of ξ. This numerical technique accurately predicts the shock wave boundary-layer interaction, which is not accounted for in Kutler's solution. Both theoretical methods provide good agreement with experimental data, except in the vicinity of the bow shock. In this region, the current numerical model does not account for the spillover of the compression side bow shock at the leading edge. By neglecting the lower surface flow influence, a much weaker leading-edge compression wave is computed due to displacement effects of the boundary layer. This very weak shock wave is clearly depicted in the density contour plot shown later in Fig. 6.

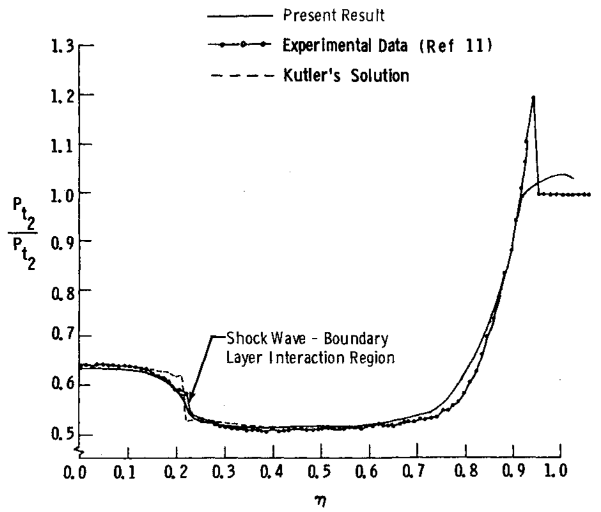

Fig. 2 Pitot pressure distribution in spanwise direction for supersonic flow above a planar delta wing, $\xi = 0.0718$.

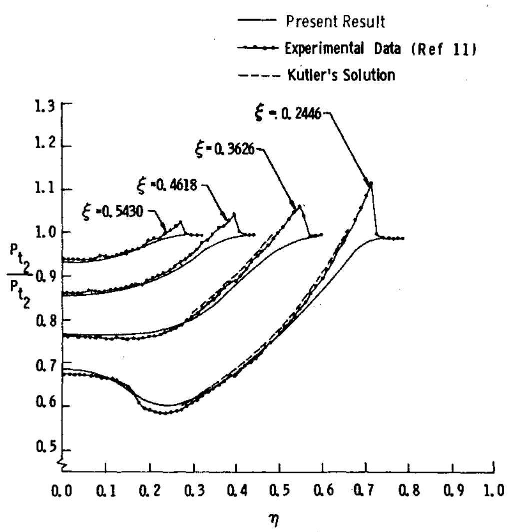

Fig. 3 Pitot pressure distribution in spanwise direction for supersonic flow above a planar delta wing.

Since the inviscid flowfield and shock wave structure are nearly conical, the velocity components in a spherical coordinate system are used to delineate the three-dimensional flowfield. The velocity vectors normal to the rays through the vertex of the delta wing are projected on the ξ,η plane as shown in Fig. 4. The relative magnitude of these vectors is illustrated for all but the lowest momentum region. The direction of these vectors is given by

$$\tan\gamma_c = (u\xi - w)/(u\eta - v) \qquad (14)$$

where γ_c is the angle measured from the positive η axis. The locus of these velocity vectors trace out "pseudo" streamlines

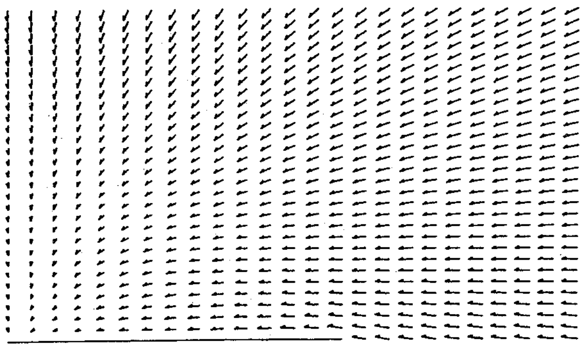

Fig. 4 Crossflow vector velocity plot as seen on spherical surface for supersonic flow above a planar delta wing, $\alpha = 12$ deg.

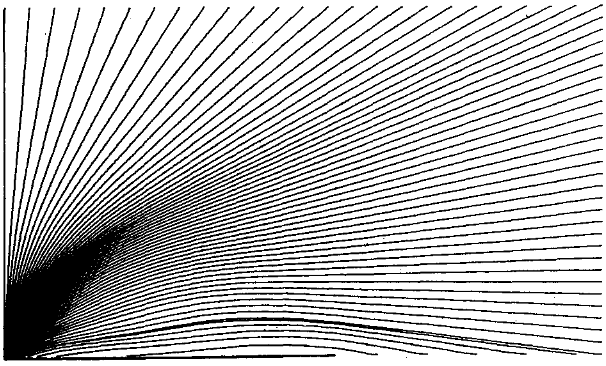

Fig. 5 Crossflow streamline plot as seen on spherical surface for supersonic flow above a planar delta wing, $\alpha = 12$ deg.

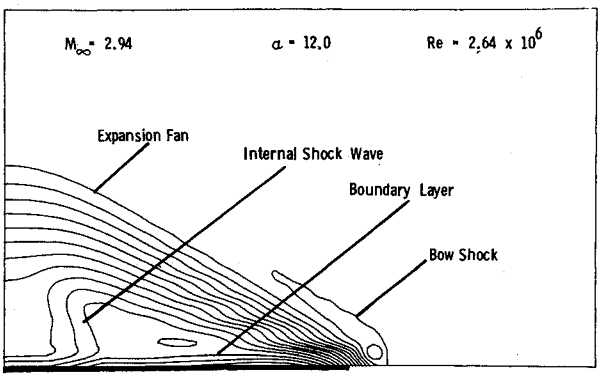

Fig. 6 Crossflow static density contour for supersonic flow above a planar delta wing.

which converge at a vortical singularity point (crossflow stagnation point) near the origin. In the unperturbed flow region (upper and right portions of Fig. 4), the conical crossflow velocity vectors point to the origin of the coordinate system. Figure 5 illustrates some of the crossflow conical streamlines (780 points). A linear interpolation technique (i.e., modified Euler-Cauchy method) was used to determine these steady-state path lines. Figure 5 shows more clearly how most of these conical streamlines converge at the vortical singularity point, even though the numerical resolution in the boundary layer is marginal. This result is consistent with the experimental observations by Bannink and Nebbeling.

The density contour in the physical y,z plane is shown in Fig. 6. This contour plot was developed by using a General Purpose Contouring Program[23] on the CDC 6600 computer. A total of 780 data points were evaluated in order to produce this figure. The internal shock wave and leading-edge expansion fan are clearly depicted as highly concentrated contour lines. These contour lines indicate that the inboard shock wave, starting perpendicularly from the wing surface, extends into the central region where the expanded flow is dominant. In this region, the internal shock weakens and eventually becomes a conical sonic line. Along the wing surface, the boundary layer is very thin and the adverse pressure gradient induced by the shock wave-boundary layer interaction is weak. No flow separation occurs at the base of the internal shock.

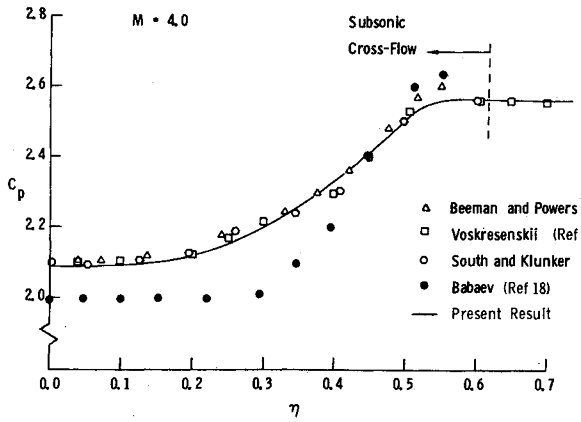

Fig. 7 Spanwise pressure distribution on compression side of planar delta wing at supersonic speeds.

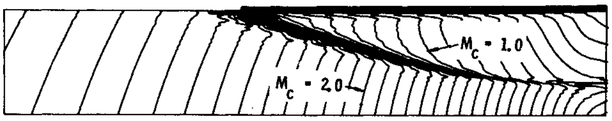

Fig. 8 Crossflow Mach number contour for supersonic flow below a planar delta wing.

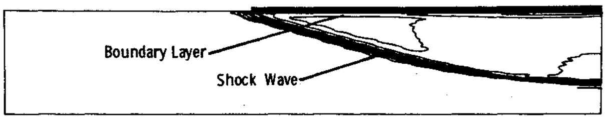

Fig. 9 Crossflow static density contour for supersonic flow below a planar delta wing.

Compression Side Flowfield Solution

In this study, only one compression side flowfield case was computed. The freestream conditions chosen for this calculation are

$$M_\infty = 4.0 \qquad \Lambda = 50$$

$$Re_x = 5.0\times 10^6 \qquad T_w = 530^\circ\mathrm{R}$$

$$Pr = 0.72 \qquad \gamma = 1.4$$

$$\alpha = 15\ \mathrm{deg} \qquad \bar{\chi} = 0.028$$

where T_w is equal to the freestream stagnation temperature. These flow conditions are identical to those used by Babaev,[18] Voskresenskii,[19] Beeman and Powers,[21] and South and Klunker[20] in their inviscid analyses.

A 26 (η)×45 (ξ) array was used in this numerical calculation. This constant step size array was identical to the lower half of the grid system shown in Fig. 1. The η step size was 0.059936 with 14 grid points on the wing surface. The ξ step size was 0.00568. The freestream boundary locations were positioned far enough from the wing surface and bow shock so as to not affect the numerical solution. The results of this calculation are shown in Figs. 7-9.

In Fig. 7, the coefficient of pressure on the lower surface of a flat delta wing is plotted for various spanwise locations. The primary area of interest in this figure is the subsonic crossflow region, where a variation in surface pressure occurs. The crossflow sonic line (as seen later in Fig. 8) serves as a dividing line between the rotational and irrotational portions of the flow. Close agreement is seen between the subsonic numerical calculations and all of the analytical solutions except Babaev's solution. In Babaev's method, an attempt is made to account for the singularity which occurs at the crossflow sonic point (on the wing surface). The analytical surface pressure distribution should exhibit a "corner" or slope discontinuity at the crossflow sonic point. However, Babaev's solution, as well as all the other analytical solutions, show a very smooth pressure distribution at this point. Most of the other analytical techniques ignored this weak singularity.

In Fig. 8, the crossflow Mach number contours based on the magnitude of the conical crossflow velocity components are shown. This figure defines the crossflow subsonic and supersonic regions and the sonic line that separates these regions. The sonic point is located at the base of the sonic line in the boundary layer or on the wing surface (inviscid solution only).

Figure 9 demonstrates that the shock wave from the leading edge to the sonic line is nearly planar. The numerical shock angle compares quite favorably with the inviscid analytical shock angle of 21.3 deg. A strong density gradient is calculated in the thin boundary-layer region, as seen by the highly concentrated density contour lines.

Total Flowfield Solution

For a total flowfield solution, a hypersonic flowfield case was selected. The freestream conditions chosen for this calculation are

$M_\infty = 10.17$ $\quad T_{0_\infty} = 1780°\mathrm{R}$

$Re_x = 3.345 \times 10^5$ $\quad P_{0_\infty} = 596$ psia

$Pr = 0.72$ $\quad \gamma = 1.4$

$\bar{\chi} = 9.4$ $\quad T_w = 1259°\mathrm{R}$

$\alpha = 15$ deg $\quad \Lambda = 75$ deg

These are the same flow conditions used by Cross[12] in his experimental study of the expansion side flowfield over a flat delta wing at hypersonic speeds.

The computational domain, as shown in Fig. 1, consisted of a 26 (η) × 120 (ξ) grid array with 75 rows of ξ grid points above the wing and 44 rows below the wing. The η step size was 0.019139 with 14 grid points on the wing surface. The ξ step size was 0.00568. The freestream boundaries (upper, lower, and right side) were located far enough from the wing surface as not to effect the numerical solutions. The incremental step sizes were selected so that no interpolation was required in order to compare experimental and numerical results. The ξ step size also resulted in at least 5 grid points in the compression side boundary layer and almost 40 grid points in the leeside centerline boundary layer. The results of these calculations are shown in Figs. 10-14.

In Fig. 10, a comparison is made between the experimental and calculated edge of the viscous region. This viscous profile is determined by evaluating the impact pressures in the ξ direction, similar to what was done in Ref. 12. It can be clearly seen that there is a progressive increase in the extent of the viscous region as the angle of attack is increased. At low angles of attack ($\alpha \leq 5$ deg), the calculated profile can be approximated by $\delta \simeq \eta^{1/2}$. This result is similar to the qualitative flow behavior noted by Rao and Whitehead[4] in their vapor screen studies. At $\alpha = 9$ deg, a centerline "trough" appears in the calculated viscous profile. This trough is generated by shock-induced vortices in the viscous region. Cross' data, for $\alpha \geq 9$ deg, show a large region of low impact pressure development along the centerline of the wing. Numerical results for $\alpha \geq 11$ deg verify this large low impact pressure region or viscous "hump" along the symmetry plane. This viscous bubble occurs as a result of shock-induced separation behind a strong leeside bow shock. The center of this viscous hump is located near the projection point of the freestream velocity vector (through the wing vertex) on the ξ,η plane.

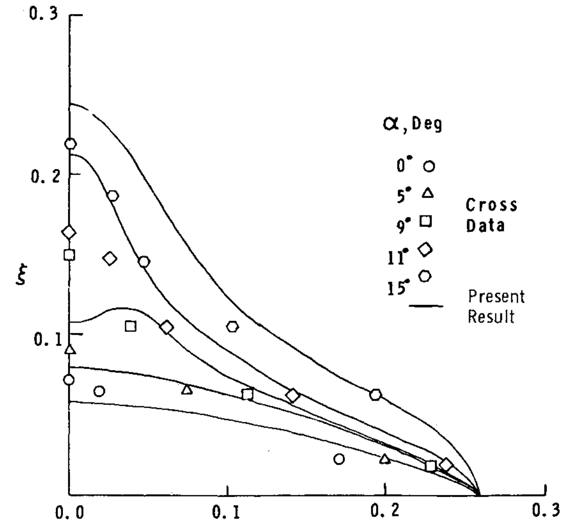

Fig. 10 Hypersonic viscous layer development as determined by impact pressure measurements.

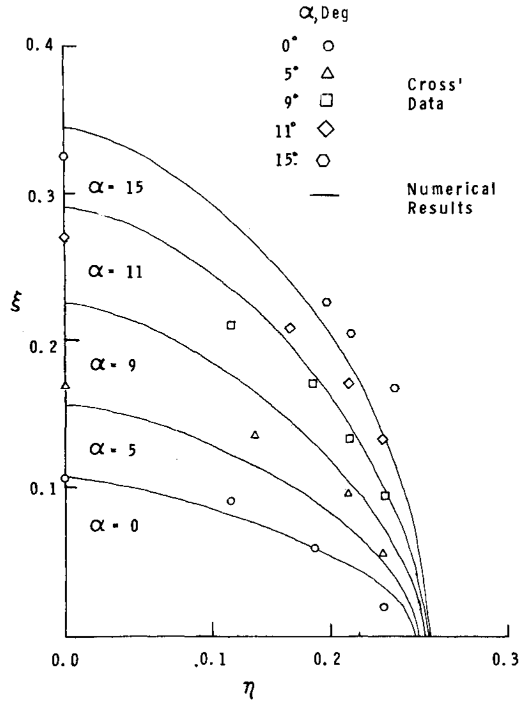

Fig. 11 Hypersonic bow shock profile above a planar aelta wing.

Figure 11 shows the bow shock location on the expansion side of the delta wing for various angles of attack. For $\eta \geq 0.1$, the calculated shock profile is slightly less than the measured shock location. This discrepancy occurs because the displacement thickness of the thin, planar delta wing is smaller than that of the actual wind-tunnel model. Along the

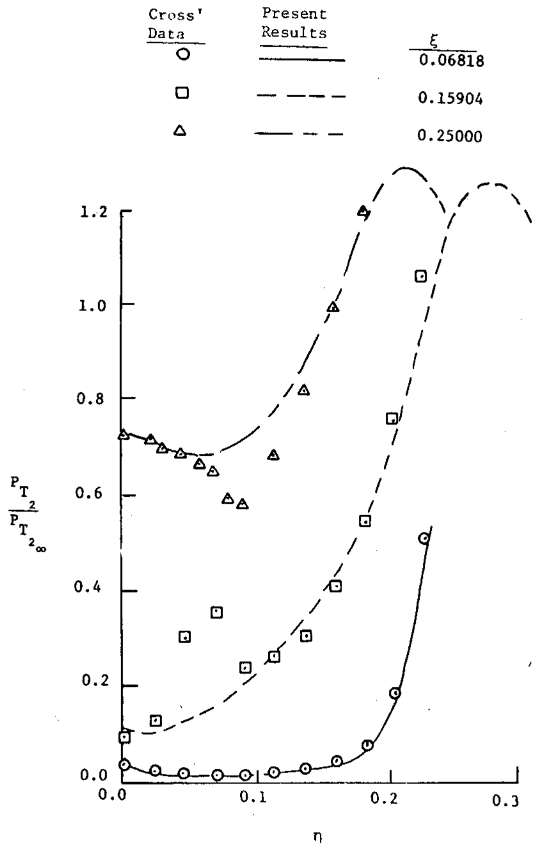

Fig. 12 Impact pressure survey on leeside of delta wing, $\alpha = 15$ deg.

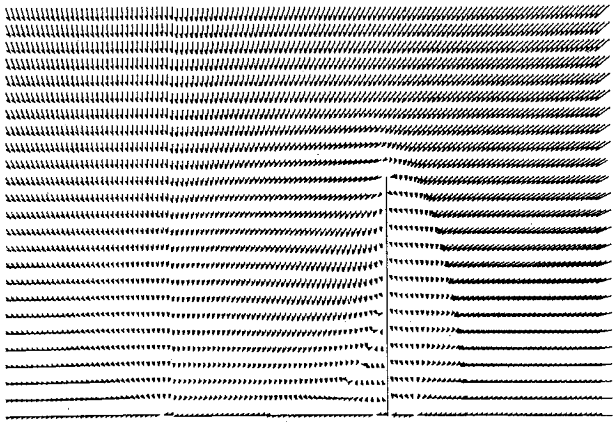

Fig. 13 Crossflow vector velocity plot as seen on spherical surface for hypersonic flow around a planar delta wing, $\alpha = 15$ deg.

plane of symmetry, good agreement is seen between the calculated and measured shock shape for $\alpha \leq 5$ deg. However, for $\alpha > 11$ deg, the numerical shock profile is slightly greater than the experimental value. This error is due to the displacement effects of the calculated boundary layer in the symmetry plane.

The spanwise impact pressure distribution for 15 deg angle of attack and various ξ positions is shown in Fig. 12. In this figure, good agreement is seen between the theory and experiment except near the centerline of the wing at $\xi = 0.15904$ and $\xi = 0.20454$. This discrepancy occurs because the calculated viscous region is slightly thicker and wider than the measured value. Good correlation is seen near the bow shock and in the inviscid region above the boundary layer.

The conical crossflow velocity vectors are shown in Fig. 13. In this figure, two vortical singularities occur near the edge of the viscous region above and below the wing surface. The crossflow separation point on the leeside of the wing is at $\eta = 0.12383$ with the experimental point at $\eta = 0.13472$. A vortex is formed in the boundary layer as a result of shock-induced boundary layer separation. This vortex is more clearly depicted in the conical streamline plot in Fig. 14. From this streamline plot it can be seen that several secondary vortices are located near the origin and very close to the wing surface on either side of the shock wave-boundary layer interaction zone. The circulation of these secondary vortices is much weaker than the primary vortex and opposite in direction. The calculation of a primary vortex in the viscous region is consistent with the experimental observations by Cross.[12]

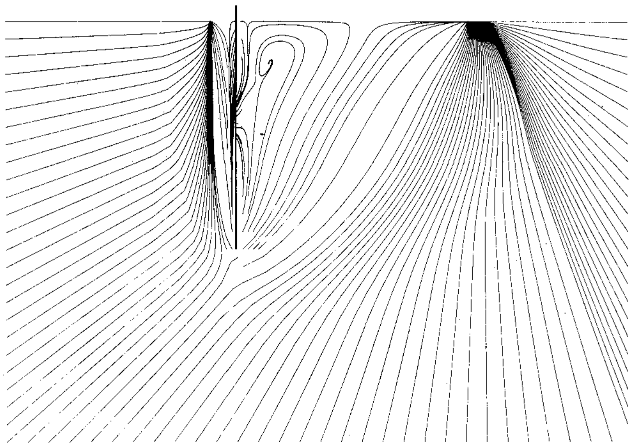

Fig. 14 Crossflow streamline plot as seen on spherical surface for hypersonic flow around a planar delta wing, $\alpha = 15$ deg.

VI. Conclusion

In conclusion, it can be seen that this numerical technique accurately predicts most of the basic elements of the flowfield. For the first time in any delta wing calculation, the shock-induced vortex development in the boundary layer and the viscous "bubble" on top of the hypersonic boundary layer can be calculated. Both the supersonic and hypersonic numerical results compare quite favorably with experimental data[11,12] as well as with several qualitative observations.[4] These numerical calculations show that a three-dimensional, supersonic and hypersonic, viscous flow around a thin delta wing can be accurately approximated by using a conical flowfield model.

References

[1] Stanbrook, A. and Squire, L. C., "Possible Types of Flow at Swept Leading Edges," *The Aeronautical Quarterly*, Vol. 15, Feb. 1964, pp. 72-82.

[2] Dunavant, J. C., Narayan, K. Y., and Walberg, G. D., "A Survey of Leeside Flow and Heat Transfer on Delta Planform Configurations," AIAA Paper 76-118, Jan. 1976.

[3] Squire, L. C., "Flow Regimes over Delta Wings at Supersonic and Hypersonic Speeds," *The Aeronautical Quarterly*, Vol. 27, Feb. 1976, pp. 1-14.

[4] Rao, D. M. and Whitehead, Jr. A. H., "Leeside Vortices on Delta Wings at Hypersonic Speeds," *AIAA Journal*, Vol. 10, Nov. 1972, pp. 1458-1465.

[5] Fowell, L. R., "Exact and Approximate Solutions for the Supersonic Delta Wing," *Journal of the Aeronautical Sciences*, Vol. 23, Aug. 1956, pp. 709-720.

[6] Babaev, D. A., "Numerical Solution of the Problem of Flow Around the Upper Surface of a Triangular Wing by a Supersonic Stream," *USSR Computational Mathematics and Mathematical Physics*, Vol. 2, 1962, pp. 296-308.

[7] Hui, W. H., "Supersonic and Hypersonic Flow with Attached Shock Waves over Delta Wings," *Proceedings of the Royal Society of London, Ser. A*, Vol. 325, Nov. 1971, pp. 251-268.

[8] Voskresenskii, G. P., "Numerical Solution of the Problem of the Flow of a Supersonic Gas Stream over the Upper Surface of a Delta Wing in the Expansion Region," *Zhurnal Prikladnoi Mekhaniki i Tekhinicheskoi Fiziki*, Vol. 6, Nov.-Dec. 1973, pp. 76-81.

[9] Kutler, P., "Computation of Three-Dimensional, Inviscid Supersonic Flows," *Lecture Notes in Physics*, edited by H. T. Wirz, Springer-Verlag, Heidelberg, Germany, 1975.

[10] McRae, D. S., "A Numerical Study of Supersonic Viscous Cone Flow at High Angle of Attack," AIAA Paper 76-77, June 1976.

[11] Bannink, W. J. and Nebelling, C., "An Experimental Investigation of the Expansion Flow Field over a Delta Wing at Supersonic Speed," Technological University Delft, Delft, The Netherlands, Rept. VTH-167, Sept. 1971.

[12] Cross, E. J., "Experimental and Analytical Investigation of the Expansion Flow Field over a Delta Wing at Hypersonic Speeds," Aerospace Research Laboratories, ARL 68-0027, Wright-Patterson Air Force Base, Ohio, Aug. 1971.

[13] Spurlin, C. J., "Expansion Side Flow Field Impact Pressure Surveys of a 75-Deg Delta Wing at Mach Number 10, Arnold Engineering Development Center, AEDC-TR-68-58, Arnold Air Force Station, Tenn., ADEC-TR-68-58, June 1968.

[14] Barber, E. A., "Some Experiments on Delta Wings in Hypersonic Flow," *AIAA Journal*, Vol. 4, Jan. 1966, pp. 72-83.

[15] MacCormack, R. W., "The Effects of Viscosity in Hypervelocity Impact Cratering," AIAA Paper 69-354, April 1969.

[16] MacCormack, R. W. and Baldwin, B. S., "A Numerical Method for Solving the Navier-Stokes Equations with Applications to Shock Boundary-Layer Applications," AIAA Paper 75-1, 1975.

[17] Tannehill, J. C., Holst, T. L., and Rakich, J. V., "Numerical Computations of Two-Dimensional Viscous Blunt Bdoy Flows with an Impinging Shock," *AIAA Journal*, Vol. 14, Feb. 1976, pp. 204-211.

[18] Babaev, D. A., "Numerical Solution of the Problem of Supersonic Flow Past the Lower Surface of a Delta Wing," *AIAA Journal*, Vol. 1, Sept. 1963, pp. 2224-2231.

[19] Voskresenskii, G. P., "Numerical Solution of the Problem of a Supersonic Gas Flow Past an Arbitrary Surface of a Delta Wing on the Compression Region," *Akademiia nauk SSR. Izvestiia. Mekhanika Zhidkosti i Gaza*, Vol. 4, 1968, pp. 134-142.

[20] South, J. C. and Klunker, E. B., "Method for Calculating Nonlinear Conical Flows," NASA SP-28, Oct. 1969.

[21] Beeman, E. R. and Powers, S. A., "A Method for Determining the Complete Flowfield Around Conical Wings at Supersonic/Hypersonic Speeds," AIAA Paper 69-646, June 1969.

[22] Bluford, G. S., "A Numerical Solution for the Supersonic and Hypersonic Viscous Flow Around Thin Planar Delta Wings," Ph.D. Dissertation, Air Force Institute of Technology, Wright-Patterson Air Force Base, Ohio, 1978; also available as AFFDL TR 78-98.

[23] "A General Purpose Contouring Progam-User's Manual," California Computer Products, Inc., Anaheim, Calif., Calcomp, April 1971.